Inverse design of grating metasurface for enhancing spontaneous emission through hyperbolic metamaterials

HAORAN MA,[1] GANG BAO,[1] JUN LAI[1] AND JUNSHAN LIN[2,*]

[1] School of Mathematical Sciences, Zhejiang University, Hangzhou, Zhejiang 310027, China
[2] Department of Mathematics and Statistics, Auburn University, Auburn, AL 36849, United States
[*]jzl0097@auburn.edu

Abstract: This work is concerned with inverse design of the grating metasurface over hyperbolic metamaterials (HMMs) in order to enhance spontaneous emission (SE). We formulate the design problem as a PDE-constrained optimization problem and employ the gradient descent method to solve the underlying optimization problem. The adjoint-state method is applied to compute the gradient of the objective function efficiently. Computational results show that the SE efficiency of the optical structure with the optimized metasurface increases by 600% in the near field. In particular, an optimal double-slot metasurface obtained by this design method enhances the SE intensity by a factor of over 100 in the observation region.

1. Introduction

Spontaneous emission (SE) arises from the interplay between a light emitter (such as quantum dot) and its surrounding environment, and the control of SE plays an important role on the functionalities of many optoelectronics devices [1]. Conventional approaches of using photonic crystals or nanocavities to modify the dielectric environment and manipulate the optical modes can successfully induce the so-called Purcell effect and collect the emitted photon at a given quantum state, but these strategies require to excite the resonances of photonic crystals or cavities, which imposes a restriction on the spectral width of the emitter [2–6].

The development of metamaterials has provided an alternative approach to control the SE within a much broader bandwidth. In particular, the hyperbolic metamaterials (HMMs) can be employed to either reduce or enhance the extraction efficiency of SE [7–12]. HMMs are a class of uniaxial anisotropic electromagnetic materials for which the axial principle component of their relative permittivity or permeability tensors attain opposite sign of the other two principal components. Such metamaterials can be realized, for instance, by alternating metal-dielectric layers or by embedding metallic wire array in a dielectric matrix by restricting free-electron motion to certain directions [7, 8]. More recently, hexagonal boron nitride (hBN), α-phase molybdenum trioxide (α-MoO_3), α-phase vanadium pentoxide (α-V_2O_5) and a few others have emerged as natural hyperbolic materials that attain opposite signs for the in-plane and out-of-plane components of the permittivity tensor [13, 14].

One of the crucial features in HMMs is its ability to support electromagnetic wave with arbitrarily large wave vectors, which is guaranteed by the hyperboloidal isofrequency surface of the underlying dispersion relation [15]. When such electromagnetic modes with high momentum are excited by a quantum emitter, they can be out-coupled to the free space via a grating metasurface so as to enhance extraction efficiency for SE [7, 8, 11, 12]. The outcoupling efficiency for several different configurations of gratings have been investigated [7, 8, 11, 12], with different shapes or different grating periods. For instance, it has been shown that grating metasurfaces with the proper periodic structure can improve the light extraction performance of the quantum dots embedded in HMMs by a factor of 20 [8]. However, it is not clear what grating profile would yield the highest extraction efficiency. The goal of this work is to investigate the inverse design of the 1D grating metasurface such that the out-coupling efficiency for SE is maximized.

To this end, we formulate the underlying inverse design problem as a PDE-constrained optimization problem and develop a gradient descent method to solve the optimization problem. The method requires a small number of iterations, where at each iteration, one forward and one adjoint-state problem are solved. It is shown that the extraction efficiency of metasurface is significantly enhanced with the optimization procedure, which allows for the dramatic enhancement of SE for the optical structure as demonstrated by the numerical experiments.

2. The inverse design problem: formulation and algorithm

2.1. The mathematical model for optical scattering

The time-harmonic Maxwell's equation when a dipole is presented is given by

$$\nabla \times E = i\omega\mu H, \qquad \nabla \times H = -i\omega\epsilon E + I, \tag{1}$$

where ϵ and μ are the electric permittivity and magnetic permeability, and ω is the angular frequency. $I := \vec{p}\delta(r - r_0)$ represents the dipole source, in which the polarization vector $\vec{p}$ lies on the xy plane. We assume that the electric permittivity attains the form:

$$\epsilon = \begin{bmatrix} \epsilon_x & 0 & 0 \\ 0 & \epsilon_y & 0 \\ 0 & 0 & \epsilon_z \end{bmatrix}. \tag{2}$$

In a homogeneous isotropic medium such as gold or vacuum considered here, there holds $\epsilon_x = \epsilon_y = \epsilon_z$, while in HMMs, the axial principle component of the permittivity ϵ_x attains the opposite sign of the other two principal components ϵ_y and ϵ_z such that $\Re\epsilon_x \Re\epsilon_y < 0$ and $\Re\epsilon_x \Re\epsilon_z < 0$. Under the transverse-magnetic (TM) polarization for the electromagnetic wave with

$$E = (E_x, E_y, 0)^T, \quad H = (0, 0, H_z)^T, \tag{3}$$

the above Maxwell's equation reduces to the following Helmholtz equation for the $z-$component of the magnetic field:

$$\frac{\partial}{\partial x}\left(\frac{1}{\epsilon_y}\frac{\partial H_z}{\partial x}\right) + \frac{\partial}{\partial y}\left(\frac{1}{\epsilon_x}\frac{\partial H_z}{\partial y}\right) + k^2 H_z = (\nabla \times I)_z, \tag{4}$$

where the wavenumber $k = \omega/c$, and c is the light speed.

2.2. Optimization objectives and parameters

Fig. 1 depicts the setup for the spontaneous emission model. A dipole source is placed under the HMM layer, with an Au grating metasurface sitting on top of the HMM layer to out-couple the wave modes with high momentum. Our goal is to optimize the profile of the grating metasurface such that the out-coupling efficiency is maximized along the emission direction. We set a target region D above the grating, which is a rectangular area along the emission direction, and use the strength of the wave field in D to quantify the level of the out-coupling performance for the grating metasurface. More precisely, we denote H_z in equation (4) as u, and define an energy function J to quantify the emission efficiency of the optical structure:

$$J = \frac{1}{2}\int_D |u|^2 \, dxdy. \tag{5}$$

We use a continuous non-negative function f to represent the profile of the one-dimensional grating metasurface. Thus the optimal design problem is to solve for an optimal profile function f such that J is maximized.

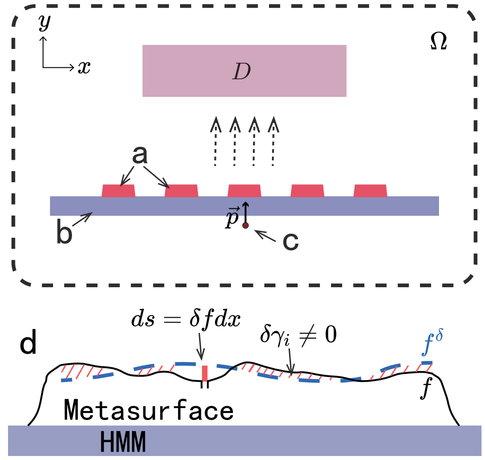

Fig. 1. The setup for the spontaneous emission model. (a) Grating metasurface. (b) Hyperbolic metamaterial (HMM) layer. (c) Emission source. (d) Perturbation of the metasurface profile on top of the HMM.

2.3. Optimization scheme

We employ the gradient descent method to minimize the functional $-J$. To this end, at each iteration we compute the gradient of J with respect to f, also known as the shape derivative, and update f along the gradient direction. To simplify the notations, we rewrite equation (4) as

$$\frac{\partial}{\partial x}\left(\gamma_1 \frac{\partial u}{\partial x}\right) + \frac{\partial}{\partial y}\left(\gamma_2 \frac{\partial u}{\partial y}\right) + k^2 u = g \quad \text{for } (x, y) \in \Omega, \tag{6}$$

where g is the source, $\gamma_1 = 1/\epsilon_x$ and $\gamma_2 = 1/\epsilon_y$. For any test function v with compact support in Ω, an integration by parts leads to

$$\int_\Omega \gamma_1 \frac{\partial u}{\partial x}\frac{\partial \bar{v}}{\partial x} + \gamma_2 \frac{\partial u}{\partial y}\frac{\partial \bar{v}}{\partial y} - k^2 u\bar{v}\, ds = -\int_\Omega g\bar{v}\, ds. \tag{7}$$

In the above, $\bar{z}$ represents the complex conjugate of z. To derive the gradient of J with respect to f, we perturb f slightly as shown in Fig. 1(d) and denote the new grating profile, the corresponding coefficients and the scattered field as $f^\delta := f + \delta f, \gamma_i^\delta := \gamma_i + \delta\gamma_i (i = 1, 2)$ and $u^\delta := u + \delta u$, respectively. Subtracting equation (7) from its perturbed one yields

$$\begin{aligned} &\int_\Omega \gamma_1 \frac{\partial \delta u}{\partial x}\frac{\partial \bar{v}}{\partial x} + \gamma_2 \frac{\partial \delta u}{\partial y}\frac{\partial \bar{v}}{\partial y} - k^2 \delta u\bar{v}\, ds \\ &= -\int_\Omega \delta\gamma_1 \frac{\partial u^\delta}{\partial x}\frac{\partial \bar{v}}{\partial x} + \delta\gamma_2 \frac{\partial u^\delta}{\partial y}\frac{\partial \bar{v}}{\partial y}\, ds. \end{aligned} \tag{8}$$

Now let us introduce the adjoint-state equation

$$\frac{\partial}{\partial x}\left(\bar{\gamma_1} \frac{\partial u^*}{\partial x}\right) + \frac{\partial}{\partial y}\left(\bar{\gamma_2} \frac{\partial u^*}{\partial y}\right) + k^2 u^* = u\chi_D \quad \text{for } (x, y) \in \Omega, \tag{9}$$

where χ_D is the characteristic function of D such that $\chi_D = 1$ when $x \in D$ and $\chi_D = 0$ otherwise. For any test function v that is compactly supported in Ω, u^* satisfies

$$\int_\Omega \bar{\gamma_1} \frac{\partial u^*}{\partial x}\frac{\partial \bar{v}}{\partial x} + \bar{\gamma_2} \frac{\partial u^*}{\partial y}\frac{\partial \bar{v}}{\partial y} - k^2 u^*\bar{v}\, ds = -\int_D u\bar{v}\, ds. \tag{10}$$

Let $v = u^*$ in (8) and $v = \delta u$ in (10), we arrive at

$$\begin{aligned}
\delta J &= J(f^\delta) - J(f) \\
&= \Re \int_D u\overline{\delta u}\, ds + O(||\delta u||^2) \\
&= \Re \int_\Omega \delta\gamma_1 \frac{\partial u^\delta}{\partial x}\frac{\partial \overline{u^*}}{\partial x} + \delta\gamma_2 \frac{\partial u^\delta}{\partial y}\frac{\partial \overline{u^*}}{\partial y}\, ds + O(||\delta u||^2),
\end{aligned} \tag{11}$$

where $\Re$ denotes the real part of a complex function. Let L be the width of the grating so that f is supported in the interval $[0, L]$ and $[U]_f$ be the jump of the function U across the interface, i.e.

$$[U(x,y)]_f := \lim_{h\to 0^+} U(x, y+h) - U(x, y-h) \;\text{ for } y = f(x).$$

Then one can rewrite (11) as an integral on $[0, L]$:

$$\delta J = -\int_0^L \Re \left[\gamma\left(\frac{\partial u^\delta}{\partial x}\frac{\partial \bar{u}^*}{\partial x} + \frac{\partial u^\delta}{\partial y}\frac{\partial \bar{u}^*}{\partial y}\right)\right]_f \delta f\, dx + O(||\delta u||^2), \tag{12}$$

where $\gamma = \gamma_1 = \gamma_2$ near the interface f since the Au grating is isotropic. Therefore, to increase the objective function, we make use of the fact that $u^\delta \approx u$ and choose δf to be

$$\delta f = h\left(-\Re\left[\gamma\left(\frac{\partial u}{\partial x}\frac{\partial \bar{u}^*}{\partial x} + \frac{\partial u}{\partial y}\frac{\partial \bar{u}^*}{\partial y}\right)\right]\right), \tag{13}$$

so that $\delta J > 0$. In the above, h is the step size at each iteration.

3. Numerical experiments

3.1. Parameters and numerical solver

3.1.1. Setup for numerical simulations and model parameters

The mathematical model is solved over a finitely truncated domain shown in Fig. 2 and the specifications of the experimental model are given in Table 1. The entire region is enclosed by a perfect matched layer (PML) to eliminate the artificial reflection from the boundary [16]. We consider an hBN HMM layer with an Au grating deposited over it. A dipole source directing along the vertical direction y is placed below the hBN layer. The region D is located in the near field with a distance of 2μm above the metasurface (cf. Fig. 2 and Table 1). To quantify the emission efficiency of the structure in the far field, we choose the region Θ which is 7μm above the metasurface (cf. Fig. 2 and Table 1). We use the scattering intensity (5) defined over near-field region D instead of the far-field region Θ to perform the optimization, because the optical wave in the near field is more sensitive to the variation of the grating profile. For clarity we rename J in (5) as J_D and define J_Θ with D replaced by Θ in (5) to represent the scattering intensity in the far field. By denoting J_D^0 and J_Θ^0 as the reference scattering intensity values for a bare hBN layer, we use the relative ratios J_D/J_D^0 and J_Θ/J_Θ^0 to quantify the SE enhancement in D and Θ respectively at the presence of grating.

3.1.2. Numerical solver and regularization

We evaluate the gradient (13) of the objective function J_D by solving the scattering problem (6) and the adjoint equation (9) using the finite element method (FEM). In order to fully resolve u and u^* in the near field, the FEM mesh near the metasurface, the HMM and the emission source is much finer than the mesh in other regions. During the optimization, the profile function f may become highly oscillatory or obtain sharp corners at certain iterations. We regularize f at each iteration by using the truncated Fourier series expansion.

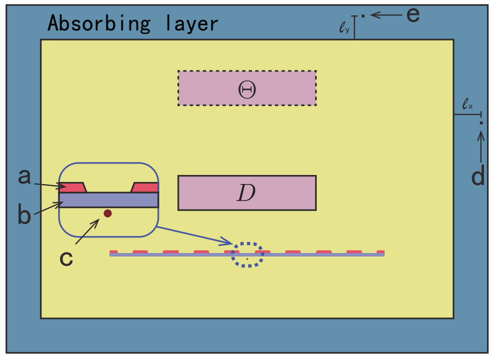

Fig. 2. The setup for computer simulation. (a) AU grating metasurface. (b) Hyperbolic metamaterial layer. (c) The dipole source. In (d) and (e), l_x and l_y denote the horizontal and vertical distances of a point (x, y) in the absorbing layer to the inner boundary of the computational domain respectively.

	L_x (μm)	L_y (μm)	D_s (μm)	ϵ_x	ϵ_y
Absorbing layer			2	$1 + 12l_x^2 i/k$	$1 + 12l_y^2 i/k$
HMM (hbN)¹	8	0.1	0.01	-8.2085+0.4571i	2.7544+0.0004i
Grating (Au)	8	f	0.11	-1637.4700+541.0360i	-1637.4700+541.0360i
Region D	4	1	2	1	1
Region Θ	4	1	7	1	1

Table 1. Parameter specifications for the model in Fig. 2. L_x and L_y denote the length and width of each region. D_s is the distance between the objects and the emission source. ϵ_x and ϵ_y are permittivity values of the materials at specified frequency.

3.2. Numerical experiments

In this section, we present three numerical experiments to illustrate the performance of the optimization algorithm. The wavelength in the first two experiments is set as 6.85 µm. In the last experiment, the optimization process is implemented over a range of frequencies.

3.2.1. Periodic structure as the initial guess

We use a periodic grating as the initial metasurface, with a period of 8/9 µm. The width of the Au cell is half of the period with a thickness of 0.08 µm. The corresponding grating profile f is given by

$$f(x) = 0.04 + 0.04\text{sign}\left(\cos\left(\frac{16}{9}\pi x\right)\right), \ x \in [0, 8]. \tag{14}$$

The optimization results and corresponding scattered field are collected in Table 2 and Fig. 3. It is observed that after four iterations, we obtain the optimized f, through which the ratio J_D/J_D^0 increases from 6 at the initial stage to 38 with the optimized grating. In other words, the optimization process increases the emission efficiency in the near field by more than 600%. Meanwhile, in the far field, J_Θ/J_Θ^0 increases from 5 to 12, as shown in Fig. 3(a). Therefore, although we utilize the near-field scattering intensity to compute the shape derivative, the

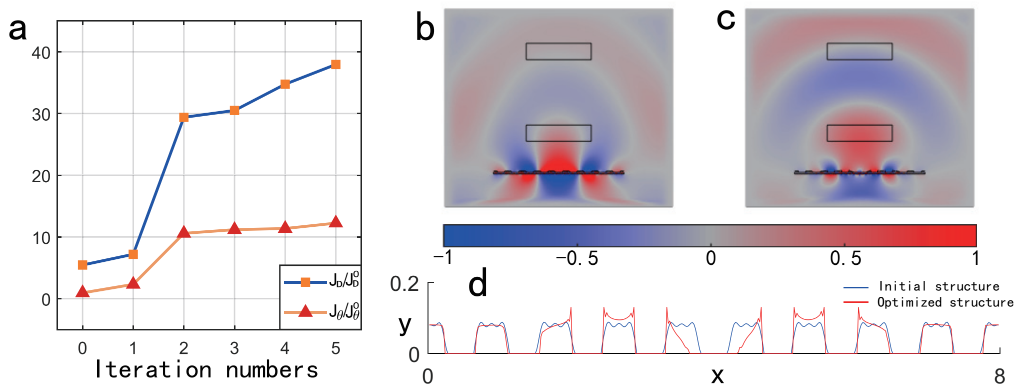

Fig. 3. (a) The growth of J_D/J_D^0 and J_Θ/J_Θ^0 during the iteration. (b) The real part of the scattered field with the initial structure. (c) The real part of the scattered field with the optimized structure. To illustrate the enhancement of scattered wave in the far field, we set the range of the colorbar from -1 to 1, noting that the wave in the near field is much stronger. The same colorbar is used in subsequent figures. (d) Initial structure vs the optimized structure.

out-coupling efficiency of the metasurface for SE is significantly enhanced in both near and far fields.

	J_D/J_D^0	J_Θ/J_Θ^0	h
Initial value	5.4508	0.9370	
Step 1	7.1902	2.3161	0.1000
Step 2	29.3840	10.5830	0.0650
Step 3	30.4933	11.1838	0.0050
Step 4	34.7516	11.3652	0.0030
Final	37.9432	12.2424	

Table 2. Optimization based on the periodic initial structure.

3.2.2. Flat metasurface as the initial guess

We use a flat Au film as the initial metasurface in this experiment. In other words, f is a constant function given by $f(x) \equiv 0.08, x \in [0, 8]$. The corresponding J_D and J_Θ are close to zero because the Au film does not couple any wave modes generated by the HMM layer, as shown in Fig. 4. The optimization algorithm performs four iterations. It is observed that J_D/J_D^0 reaches 160 and J_Θ/J_Θ^0 reaches 50 (cf. Table 3), which implies that the metasurface obtained by the optimization algorithm yields a high SE efficiency. It should be noted that significant changes of J_D and J_Θ occur at step 3. This is due to the appearance of two tiny holes in the middle of the metasurface at this iteration (cf. Fig. 4(d)). This indicates that some small holes in the grating structure may lead to a significant enhancement of SE efficiency. We explore this fact in the next experiment.

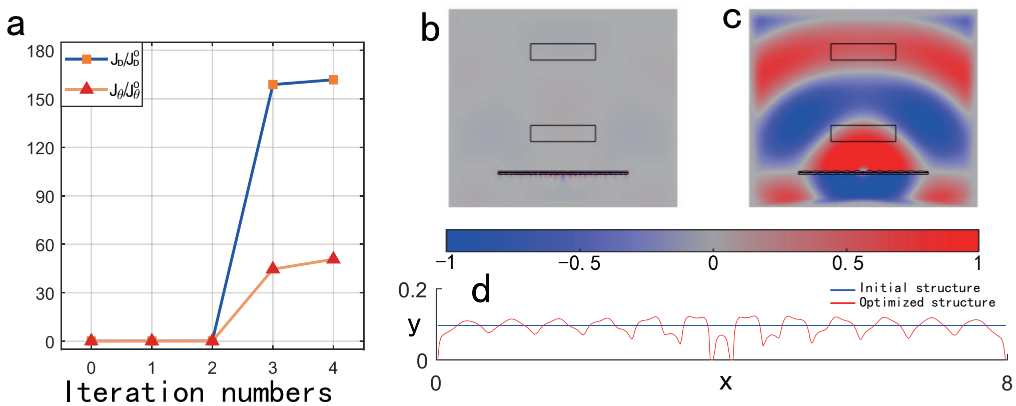

Fig. 4. (a) The growth of J_D/J_D^0 and J_Θ/J_Θ^0 during the iteration. (b) The scattered field for the initial structure. (c) The scattered field for the optimized structure. (d) Initial structure vs the optimized structure.

	J_D/J_D^0	J_Θ/J_Θ^0	h
Initial value	0.1298	0.1056	
Step 1	0.1443	0.0974	0.30000
Step 2	0.1677	0.0859	0.30000
Step 3	158.8009	44.5984	0.30000
Step 4	161.7653	50.7434	0.00037

Table 3. Optimization based on the flat metasurface

3.2.3. Double-slot grating metasurface

Based on the observation in the previous numerical experiment, we use the optimization algorithm to construct a double-slot metasurface to enhance the emission efficiency. We denote the width of the middle Au cell and the slot by α and β respectively (cf. Fig. 5(a)). We take the flat metal film as an initial guess and update α and β to maximize J_D.

Table 4 and Fig. 5 show that the optimization algorithm yields double-slot gratings with high SE efficiency at all test wavelengths. These double-slot structures allow the wave to focus on the region D. However, when the incident wavelength is short (Fig. 5(b)-(d)), the focusing effect is less significant. A possible solution is to increase the number of slots and allow each slot to change independently.

4. Conclusion

In this work, we propose an optimal design method for the grating metasurface to enhance the SE of HMMs. This method optimizes the profile of the metasurface using gradient descent via the adjoint-state method. Numerical simulations indicate that the Au grating with a periodic structure increases the SE efficiency by 600%. Moreover, a class of double-slot metasurfaces optimized by this method achieves a significant SE performance over multiple wavelengths. The method can be extended to optimize the metasurfaces in three dimensions. Another avenue to enhance the SE is to combine our algorithm with topology optimization [18] by optimizing both

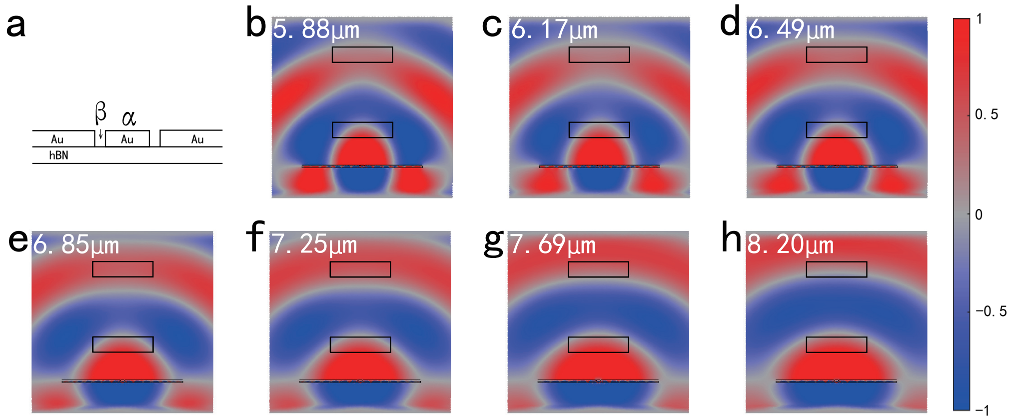

Fig. 5. The scattered field with the optimal double-slot metasurface for different wavelengths. (a) the double-slot structure with the middle Au cell width α and slot width β. (b)-(h) Scattered field of the optimized structure for different wavelengths.

λ (μm)	α (nm)	β (nm)	J_D/J_D^0	J_Θ/J_Θ^0
5.88	270	30	64.5569	59.4256
6.17	280	20	81.1792	30.2575
6.49	270	30	97.5710	38.7869
6.85	230	45	139.5458	44.4297
7.25	230	45	175.8272	47.6854
7690	220	50	191.1147	60.6277
8.20	230	45	204.1575	67.5201

Table 4. Performance of the double-slot structures.

the profile and topology of the metasurfaces. These will be reported elsewhere in the near future.

Acknowledgments

We would like to thank Siyuan Dai in Department of Mechanical Engineering at Auburn University for bringing this problem to our attention. The work of Gagn Bao and Jun Lai were supported in part by the Key Project of Joint Funds for Regional Innovation and Development (No. U21A20425) and a Key Laboratory of Zhejiang Province. Jun Lai was also supported by the "Xiaomi Young Scholars" program from Xiaomi Foundation. The work of Junshan Lin was partially supported by the NSF grant DMS-2011148.

Data Availability Statement

The data that support the findings of this study are available from the corresponding author upon reasonable request.

Disclosures

The authors declare no conflicts of interest.

References

1. T. B. Hoang, G. M. Akselrod, C. Argyropoulos, J. Huang, D. R. Smith, and M. H. Mikkelsen, "Ultrafast spontaneous emission source using plasmonic nanoantennas," Nat. communications **6**, 7788 (2015).
2. S. Fan, P. R. Villeneuve, J. Joannopoulos, and E. Schubert, "High extraction efficiency of spontaneous emission from slabs of photonic crystals," Phys. review letters **78**, 3294 (1997).
3. P. Lodahl, A. Floris van Driel, I. S. Nikolaev, A. Irman, K. Overgaag, D. Vanmaekelbergh, and W. L. Vos, "Controlling the dynamics of spontaneous emission from quantum dots by photonic crystals," Nature **430**, 654–657 (2004).
4. S. Noda, M. Fujita, and T. Asano, "Spontaneous-emission control by photonic crystals and nanocavities," Nat. photonics **1**, 449–458 (2007).
5. K. J. Russell, T.-L. Liu, S. Cui, and E. L. Hu, "Large spontaneous emission enhancement in plasmonic nanocavities," Nat. Photonics **6**, 459–462 (2012).
6. T. Tumkur, G. Zhu, P. Black, Y. A. Barnakov, C. Bonner, and M. Noginov, "Control of spontaneous emission in a volume of functionalized hyperbolic metamaterial," Appl. Phys. Lett. **99**, 151115 (2011).
7. L. Ferrari, D. Lu, D. Lepage, and Z. Liu, "Enhanced spontaneous emission inside hyperbolic metamaterials," Opt. express **22**, 4301–4306 (2014).
8. T. Galfsky, H. Krishnamoorthy, W. Newman, E. Narimanov, Z. Jacob, and V. Menon, "Active hyperbolic metamaterials: enhanced spontaneous emission and light extraction," Optica **2**, 62–65 (2015).
9. M. Noginov, H. Li, Y. A. Barnakov, D. Dryden, G. Nataraj, G. Zhu, C. Bonner, M. Mayy, Z. Jacob, and E. Narimanov, "Controlling spontaneous emission with metamaterials," Opt. letters **35**, 1863–1865 (2010).
10. D. Lu, J. J. Kan, E. E. Fullerton, and Z. Liu, "Enhancing spontaneous emission rates of molecules using nanopatterned multilayer hyperbolic metamaterials," Nat. nanotechnology **9**, 48–53 (2014).
11. K. Sreekanth, T. Biaglow, and G. Strangi, "Directional spontaneous emission enhancement in hyperbolic metamaterials," J. Appl. Phys. **114**, 134306 (2013).
12. K. V. Sreekanth, K. H. Krishna, A. De Luca, and G. Strangi, "Large spontaneous emission rate enhancement in grating coupled hyperbolic metamaterials," Sci. reports **4**, 1–7 (2014).
13. J. D. Caldwell, I. Aharonovich, G. Cassabois, J. H. Edgar, B. Gil, and D. Basov, "Photonics with hexagonal boron nitride," Nat. Rev. Mater. **4**, 552–567 (2019).
14. M. Chen, X. Lin, T. H. Dinh, Z. Zheng, J. Shen, Q. Ma, H. Chen, P. Jarillo-Herrero, and S. Dai, "Configurable phonon polaritons in twisted α-moo3," Nat. materials **19**, 1307–1311 (2020).
15. P. Huo, S. Zhang, Y. Liang, Y. Lu, and T. Xu, "Hyperbolic metamaterials and metasurfaces: fundamentals and applications," Adv. Opt. Mater. **7**, 1801616 (2019).
16. J.-P. Berenger, "A perfectly matched layer for the absorption of electromagnetic waves," J. computational physics **114**, 185–200 (1994).
17. P. Li, I. Dolado, F. Alfaro-Mozaz, A. Y. Nikitin, F. Casanova, L. Hueso, S. Vélez, and R. Hillenbrand, "Optical nanoimaging of hyperbolic surface polaritons at the edges of van der waals materials," Nano letters **17**, 228–235 (2017).
18. Y. Deng, *Adjoint Topology Optimization Theory for Nano-Optics* (Springer Singapore, 2022).